NANO LETTERS
Letter
pubs.acs.org/NanoLett

Low-Temperature Carbon Coating of Nanosized $Li_{1.015}Al_{0.06}Mn_{1.925}O_4$ and High-Density Electrode for High-Power Li-Ion Batteries

Min-Joon Lee,[†,‡,§] Eunsol Lho,[†] Peng Bai,[∥] Sujong Chae,[†] Ju Li,[*,‡,§] and Jaephil Cho[*,†]

[†] Department of Energy Engineering, School of Energy and Chemical Engineering, Ulsan National Institute of Science and Technology, Ulsan, 44919, Republic of Korea

[‡] Department of Materials Science and Engineering, [§] Department of Nuclear Science and Engineering, and [∥] Department of Chemical Engineering, Massachusetts Institute of Technology, Cambridge, Massachusetts 02139, United States

Supporting Information

ABSTRACT: Despite their good intrinsic rate capability, nanosized spinel cathode materials cannot fulfill the requirement of high electrode density and volumetric energy density. Standard carbon coating cannot be applied on spinel materials due to the formation of oxygen defects during the high-temperature annealing process. To overcome these problems, here we present a composite material consisting of agglomerated nanosized primary particles and well-dispersed acid-treated Super P carbon black powders, processed below 300 °C. In this structure, primary particles provide fast lithium ion diffusion in solid state due to nanosized diffusion distance. Furthermore, uniformly dispersed acid-treated Super P (ASP) in secondary particle facilitates lower charge transfer resistance and better percolation of electron. The ASPLMO material shows superior rate capability, delivering 101 mAh g^{-1} at 300 C-rate at 24 °C, and 75 mAh g^{-1} at 100 C-rate at −10 °C. Even after 5000 cycles, 86 mAh g^{-1} can be achieved at 30 C-rate at 24 °C, demonstrating very competitive full-cell performance.

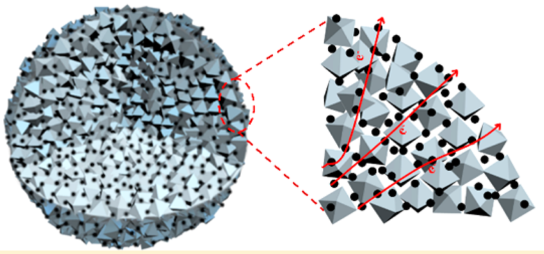
Composite with Nano LMO and Acid-treated Super P

KEYWORDS: *High power density, spinel cathode material, carbon composite, electrochemistry, lithium ion battery*

Lithium ion batteries (LIB) are the energy source of choice for electric vehicles (EVs).[1−4] The 4 V $LiM_xMn_{2-x}O_4$ (M = Li, Al, Mg, Co, Ni, and so forth) has been investigated as a potential cathode material for EVs due to its many advantages, such as high power, low cost, favorable safety, and environmental friendliness.[5−8] Especially, the spinel cathode materials (LMO) have a three-dimensional channel structure for facile lithium ions diffusion, which enables higher charge and discharge rate capabilities compared to other cathode materials, such as layered $LiCoO_2$ and olivine $LiFePO_4$. Indeed, LMO is often mixed in the cathode of Li-ion batteries in hybrid and plug-in hybrid EVs to provide a high-power component. Also, the low voltage systems LIBs (LVS, named LVS because of its lower voltage than battery of EVs, the battery with combination of $LiFePO_4$ or $LiMn_2O_4/Li_4Ti_5O_{12}$) are promising replacements of lead-acid battery in vehicle start−stop and kinetic energy recovery systems, because it can improve fuel efficiency and CO_2 emissions by up to 15%.[9,10] Vehicles with LVS are regarded as the intermediate concept between combustion engine vehicle and EVs. The LVS are lighter and smaller, and easier to design higher voltage pack (48 V) than lead-acid battery (12 V). Therefore, it can efficiently drive many electric systems in the car. The candidate of cathode materials for LVS has requirements of low cost, high safety, and high power density, which correspond to the advantage of LMO. Moreover, the electrochemical performance of LVS at low temperature (<0 °C) is important because the cell impedance would increase at low temperature leading to low charging efficiency from regenerative braking. Therefore, it has been requested to develop LMO-based cathode material with ultrafast charge/discharge properties.

Various approaches have been investigated to further enhance the kinetics of cathode materials such as nanostructuring,[11−19] coating with conductive materials,[6,20−22] and epitaxial nanostructure.[5,23−25] The nanosized materials have the advantages of shorter distance for lithium diffusion and larger surface area for charge transfer reactions.[13,26,27] However, in its as-synthesized form nanosized materials cannot fulfill the high electrode mass density (thus specific volumetric energy density) required for commercialization.[6] Secondary particles with agglomerated nanosized primary particles could be an effective solution to achieve high electrode density while preserving high rate capability if the primary nanoparticles can retain fast lithium ion insertion/extraction. However, the high rate capability of secondary particles obtained from conventional processes without good carbon enclosure of primary nanoparticles suffer from sluggish electron transport through the agglomerates, due to large amount of oxide−oxide boundaries among primary nanoparticles. It is important to replace oxide−oxide grain boundaries with oxide−carbon−

Received: March 13, 2017
Revised: April 28, 2017
Published: May 2, 2017

DOI: 10.1021/acs.nanolett.7b01076

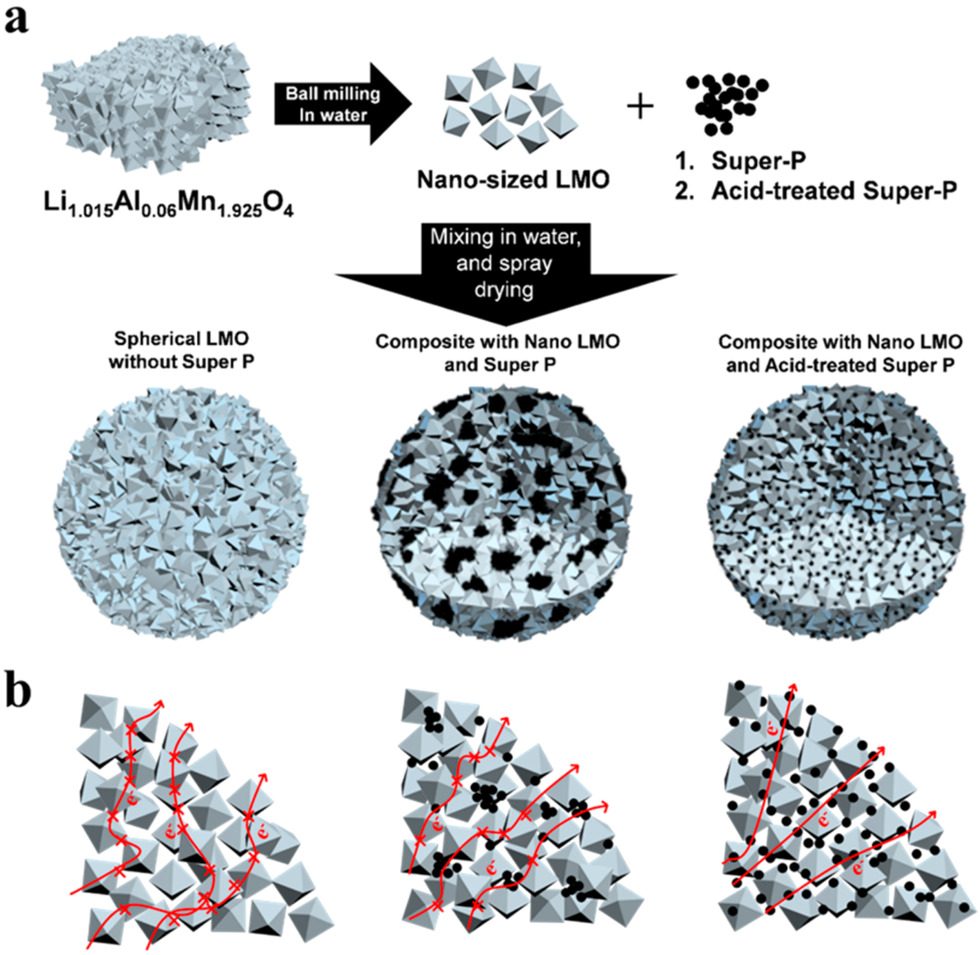

Figure 1. Schematic diagram of (a) synthesis process and composite samples with nanosized spinel and two kinds of Super P, (b) cross-section and electric-circuit configuration of three materials.

oxide phase boundaries to improve electron conduction within the secondary particle.

Carbon coating has been widely used to increase electronic conductivity.[6,28−31] Sun et al. reported carbon-coated micro-sized olivine material ($LiMPO_4$, M = Fe and/or Mn).[28] The coating layers were wrapped on the surface of every single particles, which resulted in the improved rate capability. However, carbon coating by pyrolysis of organic compounds on the LMO surface requires temperature ∼600 °C and does not give good results due to the formation of oxygen defects. For example, when sucrose-coated LMO is heated for carbonization in either air or oxygen atmosphere, carbon preferentially takes oxygen from spinel lattice to form CO_x leading to the formation of oxygen defects (Figure S1). It is also extremely difficult to conduct carbon coating on spinel materials by using chemical vapor deposition (CVD) in inert or reducing atmosphere without oxygen release. It is known that oxygen deficiency in spinel lattice worsen rate capability as well as cycling performance because the small amount of oxygen atoms in interstitial 8b site interrupts lithium ion diffusion, resulting in poor electrochemical performances.[32−34] Therefore, practical and scalable methods of carbon coating toward high rate capability without creating oxygen defects should be devised.

Herein, we wrap Super P carbon black (SP) around individual nanosized LMO primary particles and then fabricate spherical secondary particles via a water-based spray-drying process (Figure 1a). Standard SP does not have strong adhesion with LMO and the resulting dispersion is quite nonuniform. We use a dilute acid-treated Super P carbon black (denoted as ASP) to achieve better dispersion. Briefly, nanosized LMO particles were obtained by ball-milling, mixed with ASP and an appropriate amount of water, and then spray-dried at 160 °C to form spherical secondary particles with a distribution of diameters 7−40 μm, which ensure high electrode density. The acid treatment changed SP surface from hydrophobic to hydrophilic, so it could be better dispersed among nanosized spinel particles in water before spray-drying, providing facile electron pathways (Figure 1b). To the best of our knowledge, this unique strategy is first reported for LMO. The developed cathode material demonstrates extremely high charge and discharge rate capability at both low temperatures and the room temperature (RT) when paired with $Li_4Ti_5O_{12}$ (LTO) anode, matching the power of supercapacitors with superior cycling performance, even though the high-temperature performance is still lacking due to dissolution of Mn ions into the organic electrolyte.

Experimental Section. The $Li_{1.015}Al_{0.06}Mn_{1.925}O_4$ powder was synthesized with a typical sol−gel reaction. A stoichiometric amount of $Li(CH_3COO)\cdot 2H_2O$, $Al(NO_3)_3\cdot 9H_2O$, and $Mn(CH_3COO)_2\cdot 4H_2O$ was dissolved in distilled water with matching amount of citric acid as chelating agent. The aqueous solution was concentrated to produce gel, and then dried at 100 °C. The dried sample was heated at 400 °C for 5 h and then

DOI: 10.1021/acs.nanolett.7b01076
Nano Lett. 2017, 17, 3744−3751

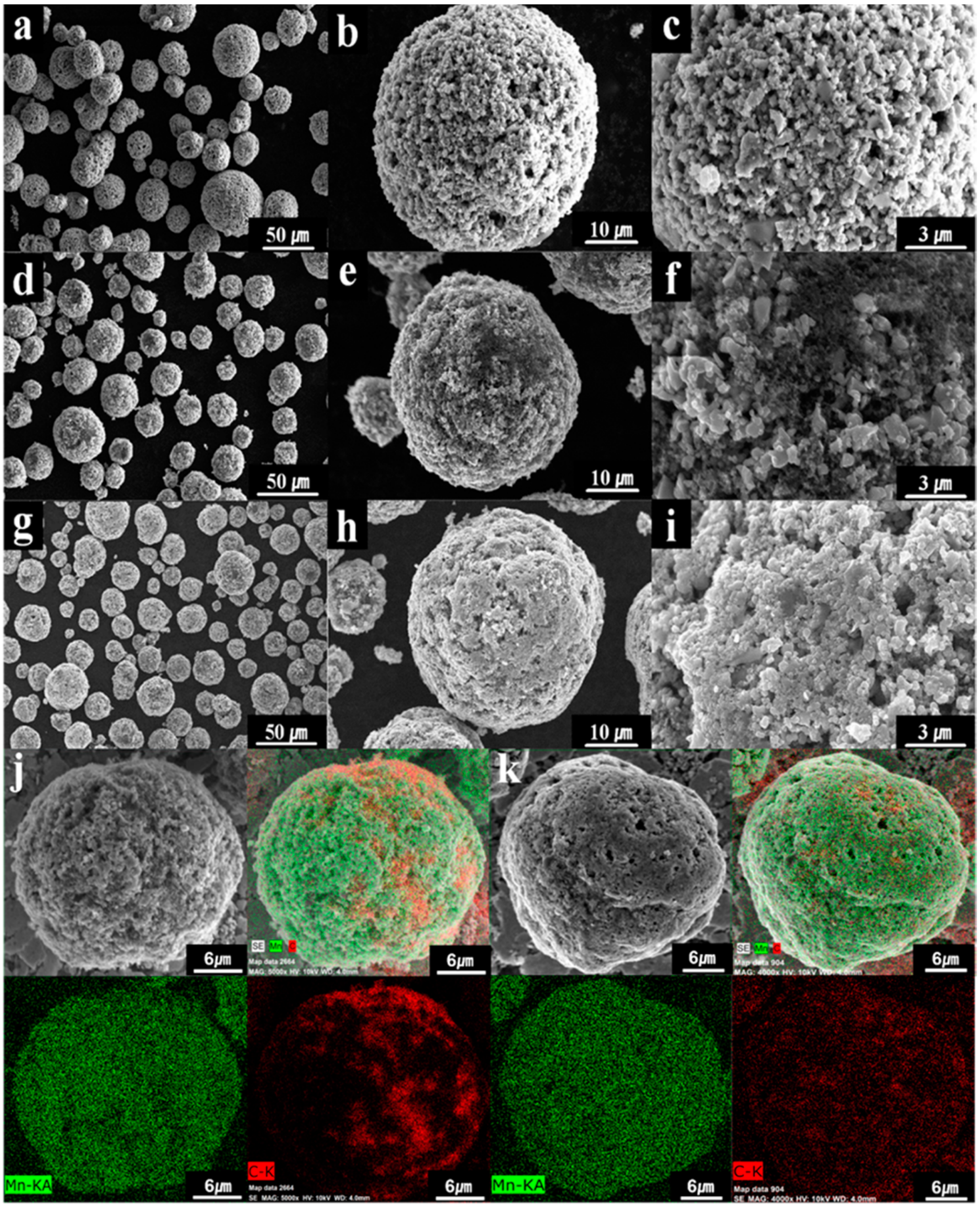

Figure 2. SEM images of (a) BLMO, (b) magnified image of (a), (c) BLMO after ball-milling, (d) SPLMO, (e,f) magnified images of (d), (g) ASPLMO, and (h,i) magnified images of (g). Energy dispersed X-ray mapping analysis of manganese and carbon of (j) SPLMO and (k) ASPLMO.

thoroughly homogenized. The homogenized powder was calcined at 770 °C for 10 h to obtain the bare spinel material. It was then ball-milled for 10 h to obtain the nanosized spinel primary particles. The acid treatment on SP was carried out with 60 mL of 0.05 M nitric acid solution and 3 g of SP. The mixture was stirred for 12 h, then filtered and washed several times to remove the nitric acid. The obtained ASP was dried at 150 °C for 24 h. The nanosized spinel powder (27 g) was mixed with ASP (3 g) and the right amount of distilled water (20 g) and were spray dried in a 30 g batch at 160 °C; then, the dried powders were heated to 300 °C in inert atmosphere to eliminate residual moisture. We denote such composite secondary particle material with acid-treated SP and nanosized LMO as ASPLMO. For comparison, we have also made a composite secondary particle material with everything the same but using untreated SP instead of ASP, and call it SPLMO. We have also made bare (i.e., single-phase) secondary spherical LMO (denoted as BLMO) microparticles and primary $Li_{1.015}Al_{0.06}Mn_{1.925}O_4$ microparticles (denoted as LMO) without the super P.

The crystalline structures were confirmed by powder X-ray diffractometer (XRD, D/MAX-2200 V, Rigaku) using Cu Kα radiation at $2\theta = 10°-80°$. The morphologies of ASPLMO, SPLMO, BLMO, and LMO were checked by using scanning electron microscopy (SEM, S-4800, HITACHI).

The four cathode electrodes were then fabricated by mixing ASPLMO/SPLMO/BLMO/LMO powder with conductive agent such as Super P and binder such as polyvinylidene

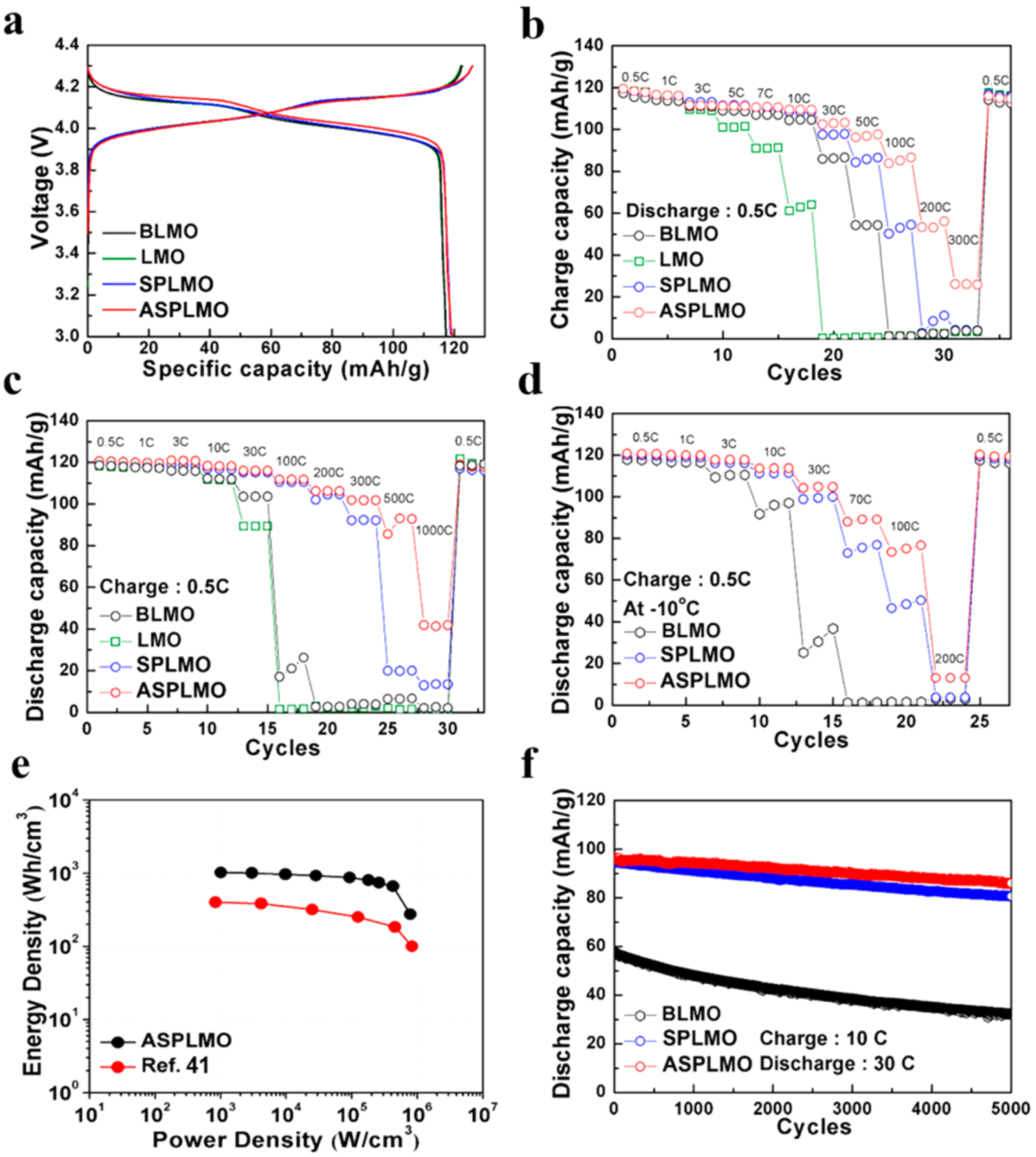

Figure 3. (a) First charge−discharge curves of BLMO, LMO, SPLMO, and ASPLMO. (b) Charge and (c) discharge capacity retention of electrodes as a function of various C rates from 0.5 to 1000 C at 24 °C. (d) Discharge rate capability of electrodes at −10 °C. (e) Ragone plot of ASPLMO and ref 41. (f) Continuous cycling results of BLMO, SPLMO, and ASPLMO at 30 C rate (10 C for charge) at 24 °C.

fluoride, respectively. To make a fair comparison, the weight ratio is 80:10:10 for ASPLMO/SPLMO electrode, and 72:18:10 for BLMO/LMO electrode, in order to make the total carbon fraction identical. The final electrode density of BLMO electrode is 2.3 g cm^{-3}, while that of ASPLMO/SPLMO electrode is 2.1 g cm^{-3}. Galvanostatic charge−discharge cycling was performed in CR2032 coin-type cell, where our cathode electrode was pitted against superabundant lithium metal in half-cell tests, or carbon-coated $Li_4Ti_5O_{12}$ anode in full cell tests with negative/positive electrode capacity ratio of only 1.03. The separator used is porous polypropylene film (Celgard 2400). The coin-type cells were assembled in an argon-filled glovebox, and 1.15 M $LiPF_6$ in ethylene carbonate/dimethyl carbonate/diethyl carbonate (3/4/3 vol % Panax Staryle) was used as the electrolyte. Before electrochemical tests, the cells were galvanostatically charged to 4.3 V at 0.1 C rate and kept at 4.3 V, until the current decreased to 0.02 C-rate, then discharged to 3.0 V versus Li/Li^+. The gravimetric capacities were calculated based on the weight of the spinel materials only (e.g., excluding ASP/SP/binder). The loading of cathode spinel materials was 4.5 mg cm^{-2} for full cell tests. Electrochemical impedance spectroscopy (EIS, IVIUM) was carried out to check impedance from 0.05 to 250 kHz frequency range in coin-type half-cells at SOC 100% in temperature bath. The obtained results were analyzed by using ZView software.

Result and Discussions. The morphologies of LMO/BLMO/SPLMO/ASPLMO samples are shown in Figure 2 and Figure S2. The LMO synthesized by sol−gel reaction and further heat treatment resulted in irregular morphology (Figure S2a,b). After ball-milling, the nanosized single crystal particles with sizes of around 100 nm could be obtained (Figure S2c). By using this nanosized powder, BLMO/SPLMO/ASPLMO were synthesized. As can be seen in Figure 2, all of the samples have spherical morphologies and their sizes are about 7−40 μm. In the case of SPLMO, the super P and nanosized LMO coexist in the secondary particle (Figure 2d−f). However, it was clearly shown that these two materials were not mixed well. On the other hand, in the case of ASPLMO it looks denser than SPLMO, and the nanosized LMO and ASP were evenly mixed in the secondary particle (Figure 2g–i). These results of SP dispersion are confirmed with the energy dispersed X-ray analysis data. As can be seen in Figure 2j, there are some regions of red dots with higher concentration in a SPLMO particle, which are obviously consistent with the agglomerated SP. On the other hand, in the case of ASPLMO the carbon elements are evenly dispersed throughout the secondary particle (Figure 2k). The reason why acid-treated SP could be evenly mixed in a secondary particle is that the surface of SP was changed from hydrophobic to hydrophilic after the acid treatment.[35,36] Therefore, it could be well dispersed in water before spray drying. It is believed that better dispersion of super P in ASPLMO would provide more facile electron pathways, especially at higher C-rate. Also the pellet densities of BLMO, LMO, SPLMO, and ASPLMO were 2.6, 2.5, 2.3, and 2.4 g cm^{-3}, respectively. The slightly reduced pellet densities compared to BLMO were attributed to the volume of SP/ASP in secondary particles (carbon has much lighter density than transition metal oxides). The crystal structures of samples were identified by XRD (Figure S3a). The patterns of three samples exhibit a well-defined cubic spinel phase of space group $Fd\bar{3}m$ without any discernible impurity peaks, which means that there is no phase transition during the synthesis process. Thermal gravimetric analysis (TGA) was carried out to confirm the amount of super P. The rate of increasing temperature is 5 °C min^{-1}. As can be seen in Figure S3b, the content of SP was 10 wt % as designed.

The electrochemical evaluations of three electrodes were performed by coin-type half cells. One C-rate was defined as 120 mA g^{-1}. Figure 3a exhibits the first charge and discharge curves of the BLMO, LMO, SPLMO, and ASPLMO between 3.0 and 4.3 V at 0.1 C-rate (12 mA g^{-1}) at 24 °C. The BLMO and LMO delivered around 117 mAh g^{-1}, while the SPLMO and ASPLMO provided slightly higher capacities about 119 mAh g^{-1} (all specific capacities were presented based on the weight of the active LMO component, where a uniform factor of 0.72 needs to be multiplied when computing the capacities of the dried slurry paste). To investigate the charge (discharge) rate capability at various currents, the cells were always fully discharged (charged) at 0.5-rate (60 mA g^{-1}) first. Figure 3b,c exhibits the capacity retentions as a function of various C-rates from 0.5 C (60 mA g^{-1}) to 300 C (36 A g^{-1}) for charge and to 1000 C (120 A g^{-1}) for discharge between 3.0 and 4.5 V at 24 °C. As can be seen in Figure 3b,c, the charge and discharge capacities of BLMO and LMO dramatically decrease with increasing current despite the relatively large amount of conductive material (18 wt %) in the electrode, whereas the composite electrodes show much improved performance, which indicates that the kinetics under high-rate operation may be governed by electron conduction inside of secondary particles. Micron-sized polycrystalline cathode particles suffer from relatively slow electron conduction compared to microsized composite particle because it consists of aggregated nanosized single crystal particles that form many grain boundaries leading to high interfacial resistance against the electron transfer through grain boundary. Also, as can be seen in Figure 3b, the SPLMO and ASPLMO had comparable capacity retentions until 10 C-rate, whereas the charge rate capability of ASPLMO was higher than that of SPLMO at higher C-rate (>10 C). The SPLMO has worse dispersion of conducting agent in secondary particles. Some regions have higher concentration of super P and others do not (Figure 2a). When a relatively low current is applied, the electrical conductivity of super P surrounding nanosized LMO in low concentration regions appears sufficient to achieve comparable performance as ASPLMO. However, when a relatively high currents are applied, the poor dispersion of super P delivered insufficient speed of electron movement, leading to higher overpotential and therefore worse charge rate capability. Consequently, the well-dispersed conductive material in ASPLMO that shows outstanding charge rate capability plays a key role in electron conduction. For example, charging at 100 C-rate achieves 73% of the initial capacity in just 26 s. The discharge rate capabilities, between 0.5 C (60 mA g^{-1}) and 1000 C (120 A g^{-1}), were also investigated after fully charging the cells at 0.5 C-rate (Figure 3c). The results exhibit a similar trend as the charge rate capability. The ASPLMO presented the best discharge rate capability among four electrodes. For example, it retained 96.2% at 30 C and 77.8% at 500 C compared to its capacity at 0.5 C, while the BLMO, LMO, and SPLMO showed worse capacity retention of 87.3%, 75.5%, and 96.2% at 30 C, and 5.4%, 2.5% and 16.6% at 500 C, respectively. Moreover, even though the electrodes show similar capacity at the same low C-rate, their working voltages are quite different during charge and discharge (Figure S4 and S5). In comparison with previous studies (Table S1), we could not find any better performances compared to ASPLMO at room temperature. The ASPLMO showed significant improvement in low temperature performance (Figure 3d) as well. At −10 °C, it exhibited superior capacity retention compared to BLMO and SPLMO from 0.5 C-rate to 200 C-rate. Many factors could affect the battery performance at low temperature (<0 °C). For example, the increased viscosity of the electrolyte could result in low ionic conductivity, and lithium diffusivity inside solid particles would also decrease at low temperatures.[24] The kinetics of electrochemical cell will deteriorate.[37,38] The hindered charge delivery that leads to increases of the charge transfer and Ohmic resistances[39,40] can be avoided by the effective structure of ASPLMO secondary particles by creating facile electron pathway to facilitate the charge delivery to and from the inside of the particles, resulting in the faster local charge transfer reaction. Consequently, the ASPLMO showed faster kinetic properties than SPLMO and BLMO at −10 °C. As shown in Ragone plot (Figure 3e), the ASPLMO exhibits a volumetric energy density of 270 Wh L^{-1} at a power density of 780 kW L^{-1}. These kinetic abilities are comparable with the layer-by-layer functionalized multiwalled carbon nanotubes (LBL-MWNTs) which is one of the highest power material showing a volumetric energy density of 250 Wh L^{-1} at a power density of 124 kW L^{-1}.[41] It is worth noting that because our sample has 2.5 times higher electrode mass density, the energy density we can achieve at the same power density of 124 kW L^{-1} is ∼1000 Wh L^{-1} (Figure 3e).

Figure 3f exhibits continuous cycling results of BLMO, SPLMO, and ASPLMO at high applied current of 30 C (10 C for charge) at 24 °C between 3.0 and 4.5 V. The cycling retention of composite electrodes is much better than that of BLMO. For example, the SPLMO and ASPLMO delivered 82.3% and 84.5%, respectively, while the BLMO could only deliver 48.1% compared to their initial capacity at 5000 cycles (Figure S6a). Also, the working voltages of the composite electrodes remain relatively constant over around 97%, whereas that of BLMO decreased to 91% (Figure S6b). It is well-known that 4 V spinel has no intrinsic material disadvantage with long cycling at room temperature.[42] Therefore, the cycling test results in this study would be strongly related to how fast electrons can be delivered.

Full cell test containing three cathodes and $Li_4Ti_5O_{12}$ anode was performed. As can be seen in Figure 4 and Figure S7, three cells show similar initial capacities of around 107 mAh g^{-1} between 0.8 and 2.9 V at 0.1 C rate, based on LMO weight. The reduced capacity compared to half-cell is obviously due to irreversible capacity of $Li_4Ti_5O_{12}$. The full cell results present similar trends with half-cell data.

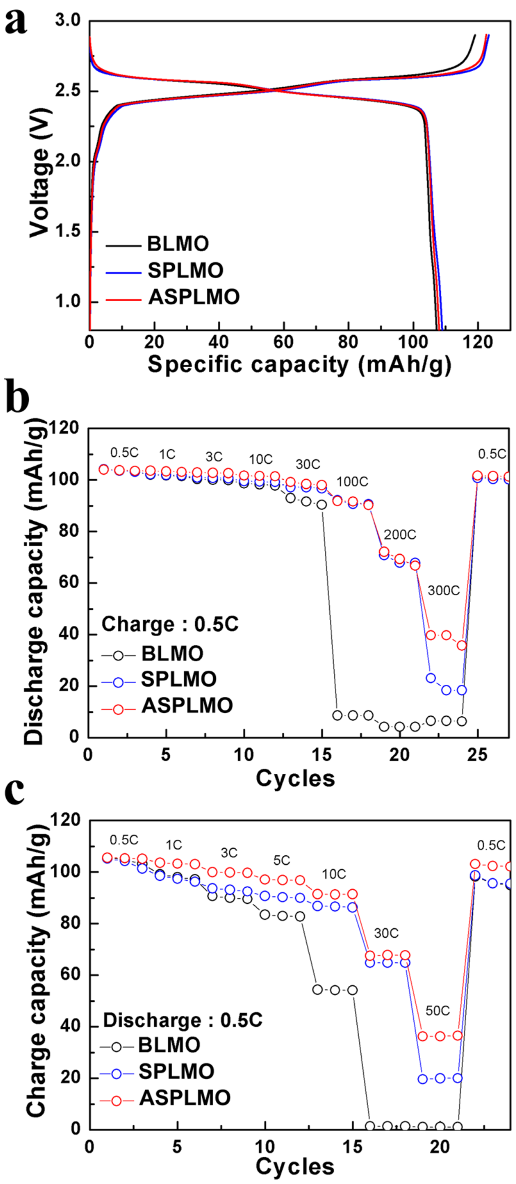

Figure 4. (a) Formation of full cell test results of BLMO, SPLMO, and ASPLMO at 0.1 C at 24 °C. (b) Discharge and (c) charge capacity retention of full cells as functions of various C rate at 24 °C. The mass loading and initial areal capacities of the $Li_4Ti_5O_{12}$ (LTO) anode and our cathode candidates are carefully matched in these full cells to achieve near-balance, with anode/cathode initial areal capacity ratio of 1.03.

In order to figure out what caused the better performances of composite electrodes, we performed electrochemical impedance spectroscopy (EIS). It was carried out at various temperature from 25 to 5 °C. All the measurements were done to cells that had been charged at 5 C to 100% SOC. As can be seen in Figure 5 with decreasing temperature, the total impedance of the three electrodes steeply increased. The BLMO electrode showed slightly higher impedance than composite electrodes at room temperature, whereas it exhibited 60% higher impedances at the lower temperatures, giving the worst low-temperature performance results (Figure 3d). Also the impedance of ASPLMO is slightly lower than that of SPLMO. The activation energies (E_a) for charge transfer resistance R_{ct} (read from the horizontal diameter of the semicircle) were calculated by using Arrhenius eq (Figure 5d).[43,44] The values of BLMO, SPLMO, and ASPLMO were 68.1, 55.7, and 51.9 kJ mol^{-1}, respectively. The lower activation barrier indicates a faster charge transfer reaction kinetics leading to higher performances at lower and lower temperatures. This is likely due to higher electronic coupling strength between the electron supplier and the receiver[45] due to better contact between electron source (carbon), ion source (liquid), and ion sink (oxide), yielding a higher exchange reaction current by more intimate contact of carbon in ASPLMO.[45]

The polarizations of three electrodes were measured by means of galvanostatic intermittent titration technique (GITT). A constant current of 3 C rate (360 mA g^{-1}) was applied for 90 s and then rested for 60 min to relax the cell voltage alternately to drive charge and discharge. As can be seen in Figure S8, the composite electrodes showed much lower overpotential throughout the entire state of charge (SOC) and depth of discharge (DOD). Also the polarization of ASPLMO is smaller than that of SPLMO. It is believed that the bottleneck for fast charge and discharge must be the electron delivery in this study, consisting of both long-range percolating transport of electrons R_{long}, and short-range charge transfer resistance R_{ct} (characterizing the local redox reaction of Li-ion with solvation shell (liquid), breaking its solvation shell near carbon and simultaneously capturing an electron from carbon, turning into a neutral $Li^+{-}Mn^{3+}$ polaron that lives and diffuses in the solid). $R_{long} + R_{ct}$ can be measured from the vertical jumps of the voltage in Figure S8e,f immediately after the current is imposed/stopped, which is a majority of the total voltage rise/drop in BLMO. The time constant of the subsequent smoother voltage change can be attributed to the diffusion of neutral $Li^+{-}Mn^{3+}$ inside LMO. When relatively high currents are applied, $Li^+{-}Mn^{3+}$ will be accumulated near the surface in the electrode material, producing a concentration gradient of $Li^+{-}Mn^{3+}$ that extends inside material. During the rest time, the concentration gradient will be reduced by $Li^+{-}Mn^{3+}$ diffusion inside the electrode, which leads to decreasing (charge) and increasing (discharge) voltages (Figure S8e−h). The fact that the time constants of this smooth voltage change in BLMO, SPLMO, and ASPLMO are approximately the same is consistent with this interpretation because the carbon coating should not affect $Li^+{-}Mn^{3+}$ transport in the interior. Consequently, the best rate capability is ascribed to the lowest $R_{long} + R_{ct}$ due to lowest activation energy for charge transfer reaction (quality of contact) and better percolation of electron paths (more uniform dispersion) in carbon black.

Conclusion. We have successfully synthesized microsized composite secondary particles consisting of nanosized spinel individually wrapped with Super P with minimal loss of electrode density. The acid treatment was carried out to change the state of carbon surface from hydrophobic to hydrophilic. Therefore, SP could be evenly distributed in a secondary particle when the water based solution was spray-dried, which was confirmed by EDX analysis. As a result, the well mixed

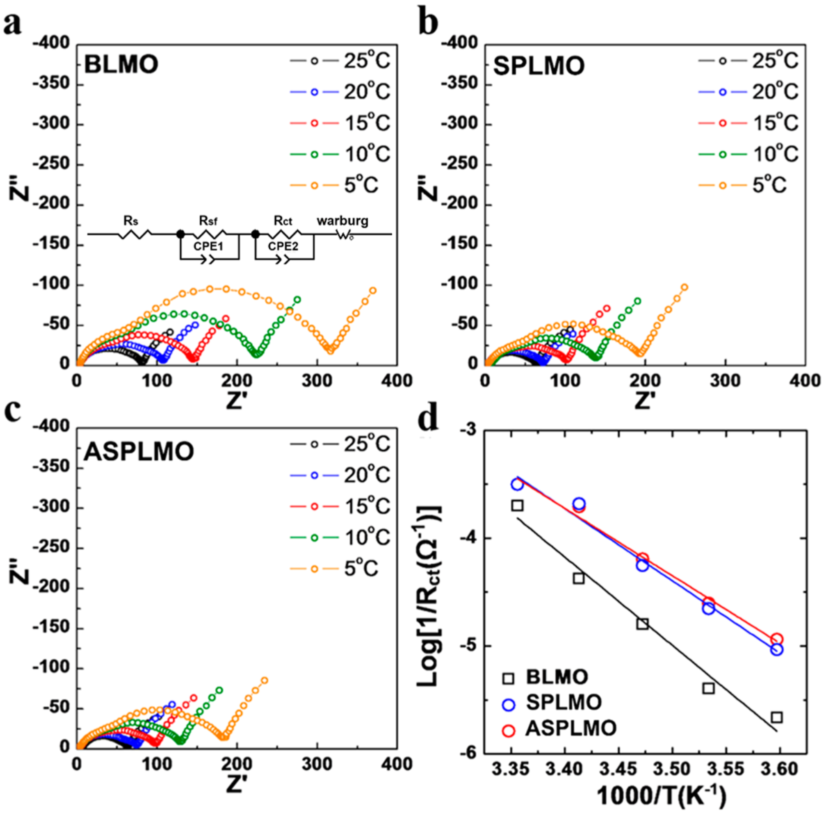

Figure 5. Nyquist plot of (a) BLMO, (b) SPLMO, and (c) ASPLMO as a function of temperatures from 25 to 5 °C. Inset of (a) shows proposed equivalent circuit comprising of resistors (R), constant phase elements (CPE). (d) Arrhenius plots of the charge-transfer resistance for BLMO, SPLMO, and ASPLMO.

acid-treated SP was able to provide more facile electron delivery compared to spherical bare spinel and composite with pristine SP. The newly developed material showed outstanding lithium ions insertion/extraction properties at −10 °C as well as 24 °C. The reasons are attributed to (1) fast lithium ion diffusion in solid state due to nanosized primary particles, (2) lower activation energy for charge transfer reaction owing to more intimate local contact, and (3) well-dispersed conductive materials, giving better global percolation of electrons. We believe that this concept can provide a direct path to improving battery performances in vehicles and even grid-scale energy storage.

■ ASSOCIATED CONTENT

Ⓢ Supporting Information

The Supporting Information is available free of charge on the ACS Publications website at DOI: 10.1021/acs.nanolett.7b01076.

> Supporting results (XRD, SEM images, TGA result), supporting electrochemical data (voltage profile, capacity retention in cycling, working voltage change, GITT results) (PDF)

■ AUTHOR INFORMATION

Corresponding Authors

*E-mail: (J.C.) jpcho@unist.ac.kr.
*E-mail: (J.L.) liju@mit.edu.

ORCID

Ju Li: 0000-0002-7841-8058

Author Contributions

M.-J.L. proposed the concept, designed the experiments, carried out the main experiments. E.L. assisted with the sample preparation and performed the electrochemical test. P.B. and J.L. assisted with the interpretation of electrochemical analysis. S.C. designed the schematic diagram. M.-J.L., J.C., and J.L. cowrote the manuscript.

Notes

The authors declare no competing financial interest.

■ ACKNOWLEDGMENTS

This work was supported by Samsung Research Funding and Incubation Center of Samsung Electronics under Project Number SRFC-TA1603-01 (Ulsan National Institute of Science and Technology) and NSF ECCS-1610806 (Massachusetts Institute of Technology).

■ REFERENCES

(1) Choi, N.-S.; Chen, Z.; Freunberger, S. A.; Ji, X.; Sun, Y.-K.; Amine, K.; Yushin, G.; Nazar, L. F.; Cho, J.; Bruce, P. G. *Angew. Chem., Int. Ed.* **2012**, *51*, 9994−10024.

(2) Lee, K. T.; Jeong, S.; Cho, J. *Acc. Chem. Res.* **2013**, *46*, 1161−1170.

(3) Thackeray, M. M.; Wolverton, C.; Isaacs, E. D. *Energy Environ. Sci.* **2012**, *5*, 7854−7863.

(4) Liu, W.; Oh, P.; Liu, X.; Lee, M.-J.; Cho, W.; Chae, S.; Kim, Y.; Cho, J. *Angew. Chem., Int. Ed.* **2015**, *54*, 4440−4457.

(5) Li, J.; Zhu, Y.; Wang, L.; Cao, C. *ACS Appl. Mater. Interfaces* **2014**, *6*, 18742−18750.

(6) Lee, S.; Cho, Y.; Song, H.-K.; Lee, K. T.; Cho, J. *Angew. Chem., Int. Ed.* **2012**, *51*, 8748−8752.

(7) Jeong, M.; Lee, M.-J.; Cho, J.; Lee, S. *Adv. Energy Mater.* **2015**, *5*, 1500440.
(8) Lee, H.-W.; Muralidharan, P.; Ruffo, R.; Mari, C. M.; Cui, Y.; Kim, D. K. *Nano Lett.* **2010**, *10*, 3852−3856.
(9) Samsung SDI. http://www.samsungsdi.com/automotive-battery/battery-application.html.
(10) Bosch Mobility Solutions. http://products.bosch-mobility-solutions.com/en/de/powertrain/powertrain_systems_for_passenger_cars_1/electric_and_hybrid/low_voltage_hybrid_systems/low_voltage_hybrid_systems.html.
(11) Kim, J.-S.; Kim, K.; Cho, W.; Shin, W. H.; Kanno, R.; Choi, J. W. *Nano Lett.* **2012**, *12*, 6358−6365.
(12) Arumugam, D.; Kalaignan, G. P. *Electrochim. Acta* **2010**, *55*, 8709−8716.
(13) Cheng, F.; Wang, H.; Zhu, Z.; Wang, Y.; Zhang, T.; Tao, Z.; Chen, J. *Energy Environ. Sci.* **2011**, *4*, 3668−3675.
(14) Hosono, E.; Kudo, T.; Honma, I.; Matsuda, H.; Zhou, H. *Nano Lett.* **2009**, *9*, 1045−1051.
(15) Xie, X.; Su, D.; Sun, B.; Zhang, J.; Wang, C.; Wang, G. *Chem. - Eur. J.* **2014**, *20*, 17125−17131.
(16) Lu, J.; Fan, X.; Zhou, C.; Liu, Z.; Zheng, F.; Lee, K. S.; Lu, L. *J. Electrochem. Soc.* **2016**, *163*, A197−A202.
(17) Kim, D. K.; Muralidharan, P.; Lee, H.-W.; Ruffo, R.; Yang, Y.; Chan, C. K.; Peng, H.; Huggins, R. A.; Cui, Y. *Nano Lett.* **2008**, *8*, 3948−3952.
(18) Ding, Y.-L.; Xie, J.; Cao, G.-S.; Zhu, T.-J.; Yu, H.-M.; Zhao, X.-B. *Adv. Funct. Mater.* **2011**, *21*, 348−355.
(19) Jiang, H.; Fu, Y.; Hu, Y.; Yan, C.; Zhang, L.; Lee, P. S.; Li, C. *Small* **2014**, *10*, 1096−1100.
(20) Sun, W.; Liu, H.; Liu, Y.; Bai, G.; Liu, W.; Guo, S.; Zhao, X.-Z. *Nanoscale* **2015**, *7*, 13173−13180.
(21) Son, J. T.; Kim, H. G.; Park, Y. J. *Electrochim. Acta* **2004**, *50*, 453−459.
(22) Huang, S.; Wen, Z.; Yang, X.; Zhu, X.; Lin, B. *Electrochem. Solid-State Lett.* **2006**, *9*, A443−A447.
(23) Kim, C.; Phillips, P. J.; Xu, L.; Dong, A.; Buonsanti, R.; Klie, R. F.; Cabana, J. *Chem. Mater.* **2015**, *27*, 394−399.
(24) Lee, M.-J.; Lee, S.; Oh, P.; Kim, Y.; Cho, J. *Nano Lett.* **2014**, *14*, 993−999.
(25) Lee, S.; Yoon, G.; Jeong, M.; Lee, M.-J.; Kang, K.; Cho, J. *Angew. Chem., Int. Ed.* **2015**, *54*, 1153−1158.
(26) Shaju, K. M.; Bruce, P. G. *Chem. Mater.* **2008**, *20*, 5557−5562.
(27) Ding, Y.-L.; Zhao, X.-B.; Xie, J.; Cao, G.-S.; Zhu, T.-J.; Yu, H.-M.; Sun, C.-Y. *J. Mater. Chem.* **2011**, *21*, 9475−9479.
(28) Sun, Y.-K.; Oh, S.-M.; Park, H.-K.; Scrosati, B. *Adv. Mater.* **2011**, *23*, 5050−5054.
(29) Oh, S.-M.; Oh, S.-W.; Yoon, C.-S.; Scrosati, B.; Amine, K.; Sun, Y.-K. *Adv. Funct. Mater.* **2010**, *20*, 3260−3265.
(30) Hsiao, K.-C.; Liao, S.-C.; Chen, J.-M. *Electrochim. Acta* **2008**, *53*, 7242−7247.
(31) Zhu, G.-N.; Liu, H.-J.; Zhuang, J.-H.; Wang, C.-X.; Wang, Y.-G.; Xia, Y.-Y. *Energy Environ. Sci.* **2011**, *4*, 4016−4022.
(32) Yoshio, M.; Noguchi, H.; Wang, H.; Wang, X. *J. Power Sources* **2006**, *154*, 273−275.
(33) Wang, X.; Nakamura, H.; Yoshio, M. *J. Power Sources* **2002**, *110*, 19−26.
(34) Kanno, R.; Kondo, A.; Yonemura, M.; Gover, R.; Kawamoto, Y.; Tabuchi, M.; Kamiyama, T.; Izumi, F.; Masquelier, C.; Rousse, G. *J. Power Sources* **1999**, *81−82*, 542−546.
(35) Kamegawa, K.; Nishikubo, K.; Kodama, M.; Adachi, Y.; Yoshida, H. *Carbon* **2002**, *40*, 1447−1455.
(36) Boehm, H. P. *Carbon* **1994**, *32*, 759−769.
(37) Smart, M. C.; Ratnakumar, B. V.; Surampudi, S. *J. Electrochem. Soc.* **1999**, *146*, 486−492.
(38) Plichta, E. J.; Hendrickson, M.; Thompson, R.; Au, G.; Behl, W. K.; Smart, M. C.; Ratnakumar, B. V.; Surampudi, S. *J. Power Sources* **2001**, *94*, 160−162.
(39) Sides, C. R.; Martin, C. R. *Adv. Mater.* **2005**, *17*, 125−128.
(40) Zhang, S. S.; Xu, K.; Jow, T. R. *J. Power Sources* **2003**, *115*, 137−140.
(41) Lee, S. W.; Yabuuchi, N.; Gallant, B. M.; Chen, S.; Kim, B.-S.; Hammond, P. T.; Shao-Horn, Y. *Nat. Nanotechnol.* **2010**, *5*, 531−537.
(42) Lee, S.; Jeong, M.; Cho, J. *Adv. Energy Mater.* **2013**, *3*, 1623−1629.
(43) Park, M.; Zhang, X.; Chung, M.; Less, G. B.; Sastry, A. M. *J. Power Sources* **2010**, *195*, 7904−7929.
(44) Okubo, M.; Mizuno, Y.; Yamada, H.; Kim, J.; Hosono, E.; Zhou, H.; Kudo, T.; Honma, I. *ACS Nano* **2010**, *4*, 741−752.
(45) Bai, P.; Bazant, M. Z. *Nat. Commun.* **2014**, *5*, 3585.

■ NOTE ADDED AFTER ASAP PUBLICATION

This paper posted ASAP on 5/10/2017. Several additional corrections were made, and the revised version was posted on 5/11/2017.

Supporting Information

Low-temperature Carbon Coating of Nanosized $Li_{1.015}Al_{0.06}Mn_{1.925}O_4$ and High-density Electrode for High-power Li-ion Batteries

Min-Joon Lee[1,2,3], Eunsol Lho[1], Peng Bai[4], Sujong Chae[1], Ju Li[2,3]*, Jaephil Cho[1]*

[1]Department of Energy Engineering, School of Energy and Chemical Engineering, Ulsan National Institute of Science and Technology, Ulsan, 44919, Republic of Korea
[2]Department of Materials Science and Engineering, Massachusetts Institute of Technology, Cambridge, Massachusetts 02139, United States
[3]Department of Nuclear Science and Engineering, Massachusetts Institute of Technology, Cambridge, Massachusetts 02139, United States
[4]Department of Chemical Engineering, Massachusetts Institute of Technology, Cambridge, Massachusetts 02139, United States

***E-mail: jpcho@unist.ac.kr (Prof. Japhil Cho), liju@mit.edu (Prof. Ju Li)**

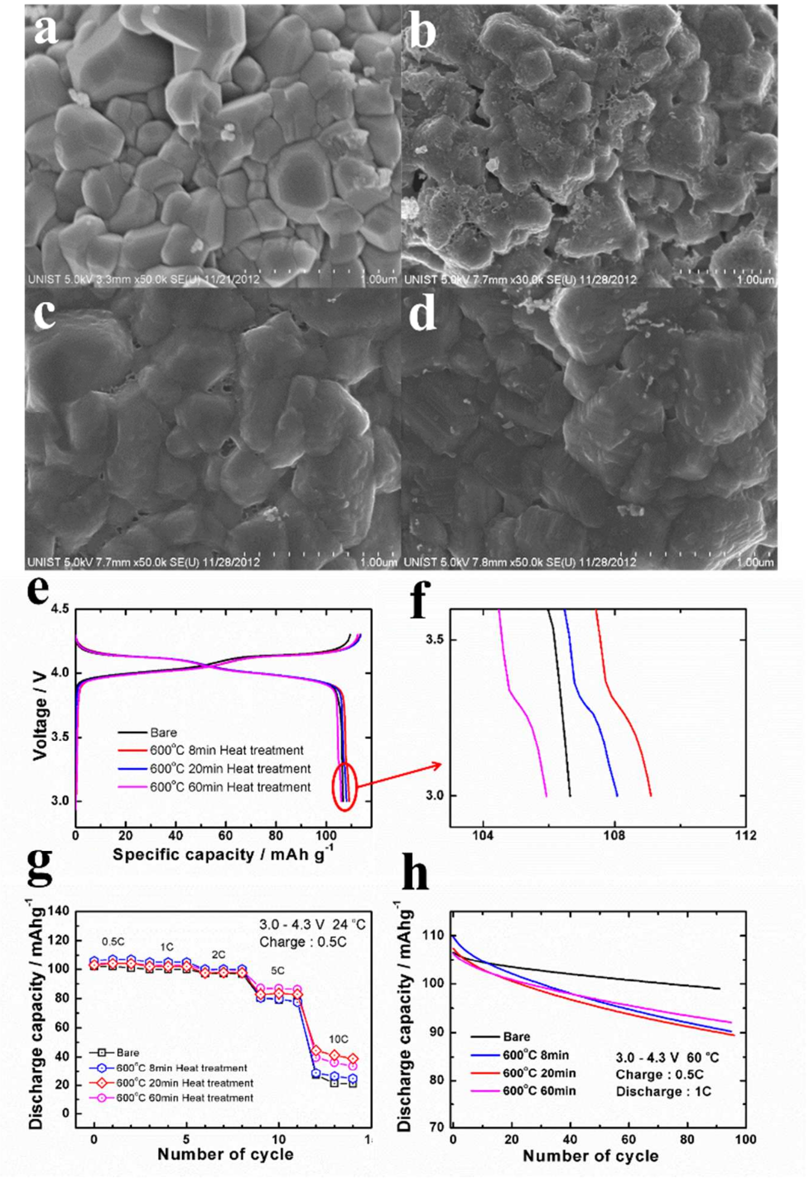

Figure S1. The carbon coating on the spinel cathode material was carried out by using sucrose-carbonization method. The coating amount of sucrose was 10 wt%. SEM images of (a) bare (b) heated at 600 °C for 8min and quenched at room temperature to minimize oxygen defects after sucrose coating, (c) 20min and (d) 60min. As can be seen in 1st cycle profiles (e) and (f), the plateau related to oxygen deficiency between 3.2 and 3.4V can be found. (g) The carbon layers can help increase rate capability slightly. However, (h) the cycling performance became worse than bare electrode due to structural instability.

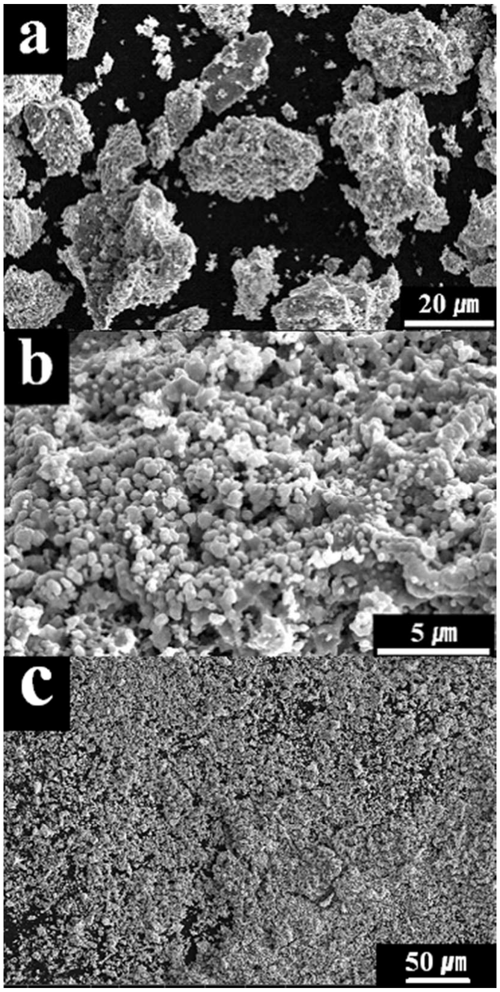

Figure S2. SEM images of (a) LMO synthesized via sol-gel reaction, (b) magnified image of (a), (c) LMO after ball-milling

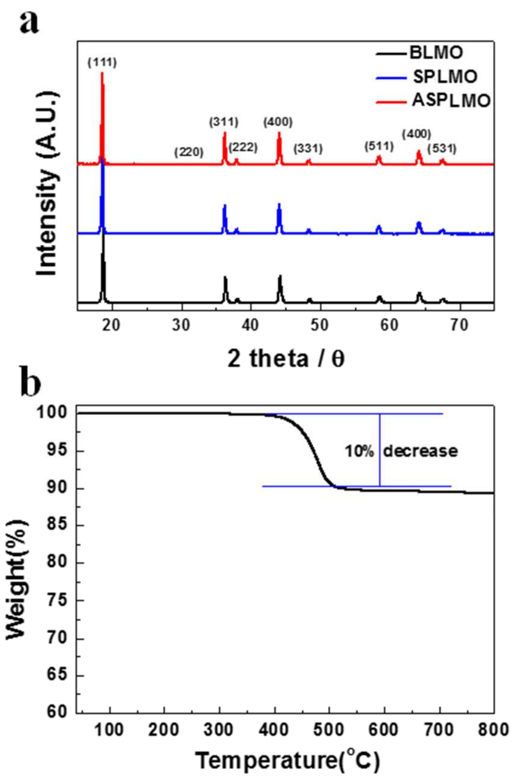

Figure S3. (a) Powder XRD patterns of BLMO, SPLMO and ASPLMO. (b) TGA results of ASPLMO with scan rate of 5 °C min^{-1}.

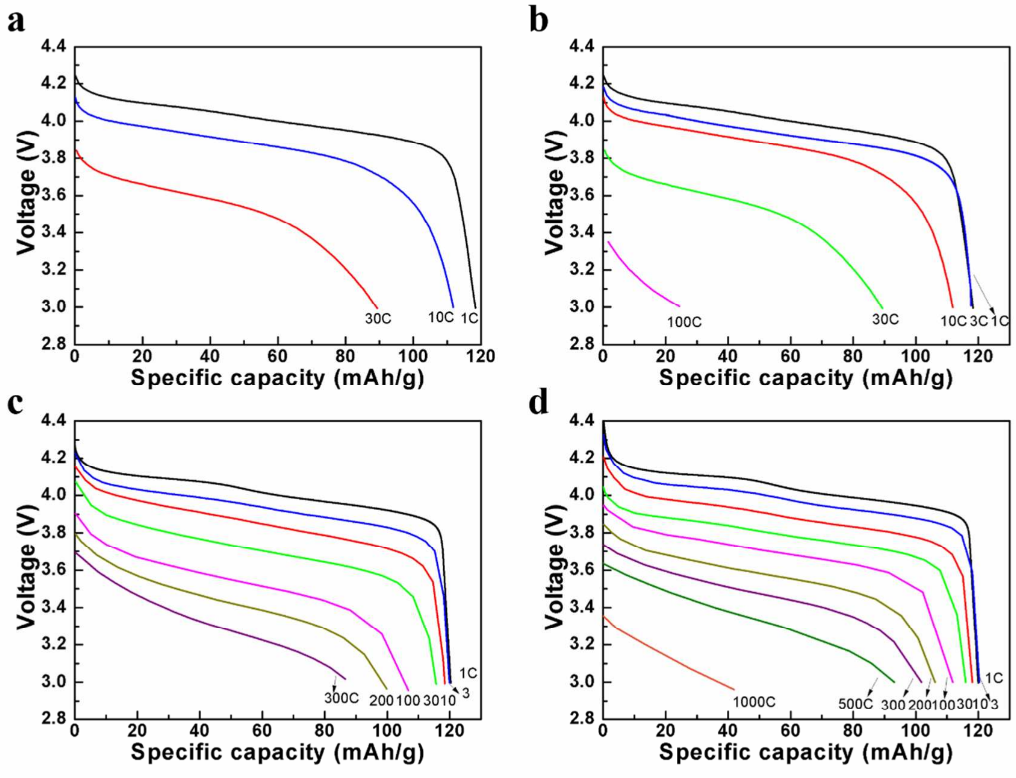

Figure S4. Discharge voltage profiles of (a) LMO, (b) BLMO, (c) SPLMO and (d) ASPLMO.

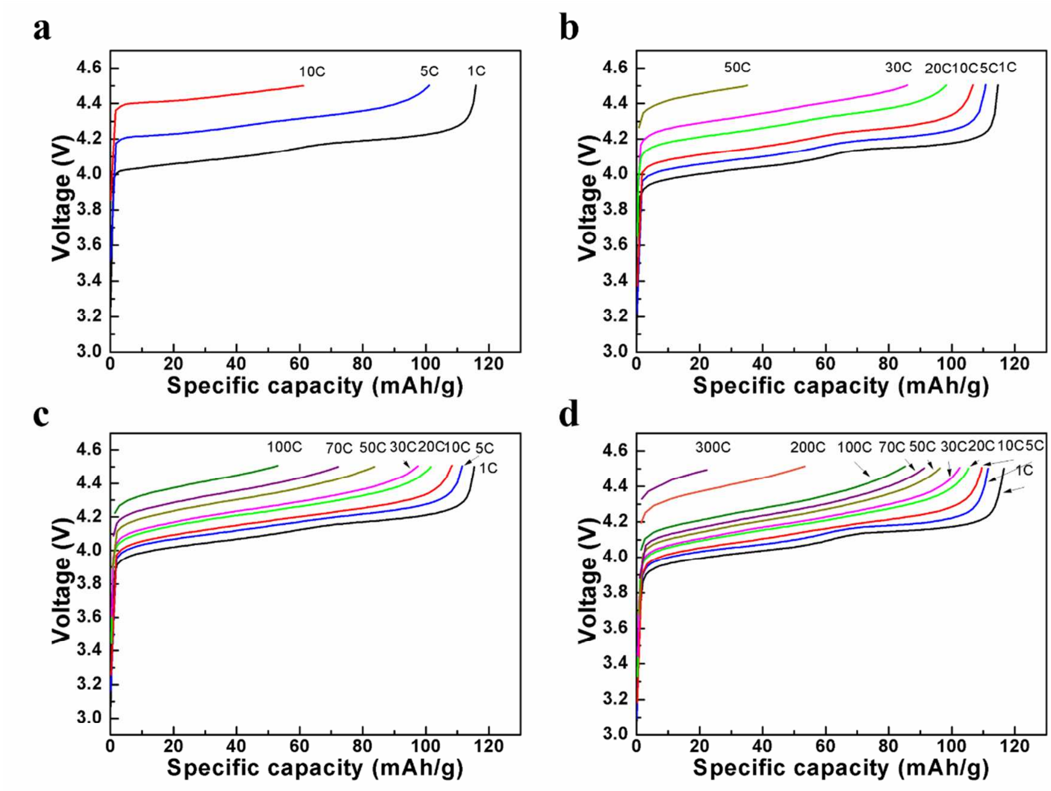

Figure S5. Charge voltage profiles of (a) LMO, (b) BLMO, (c) SPLMO and (d) ASPLMO.

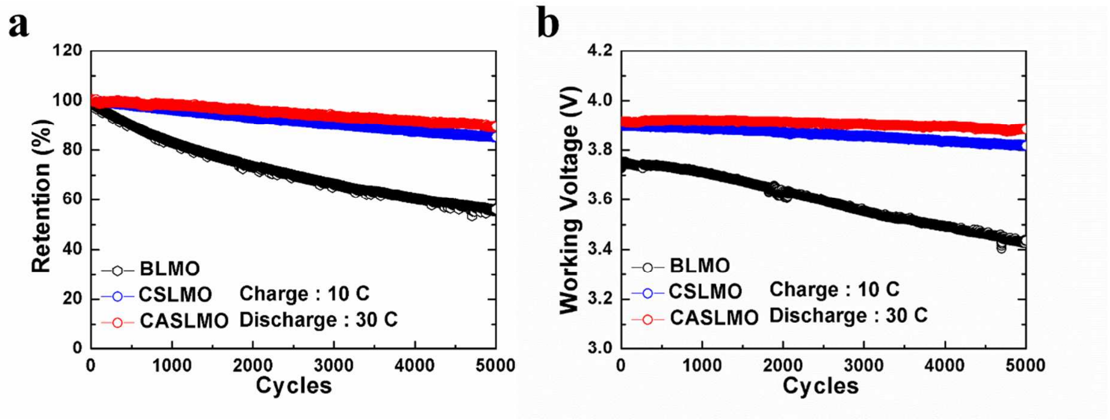

Figure S6. (a) Cycling retention and (b) Working voltage of BLMO, SPLMO and ASPLMO during continuous charge and discharge. The working voltages were calculated by using following equation. Energy density Wh/capacity Ah = working voltage V

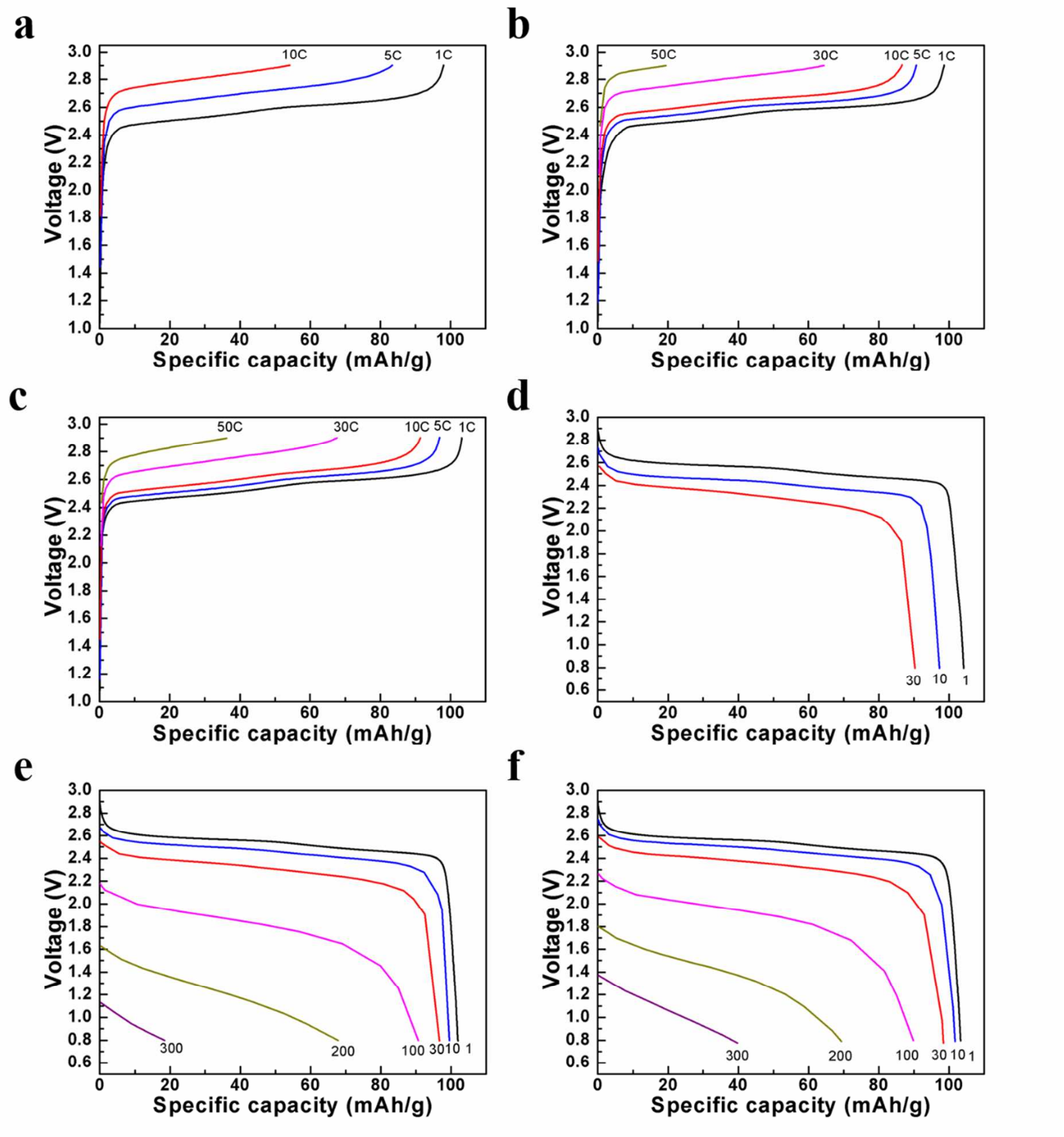

Figure S7. Charge profiles of (a) BLMO, (b) SPLMO and (c) ASPLMO, and discharge profiles of (d) BLMO, (e) SPLMO and (f) ASPLMO.

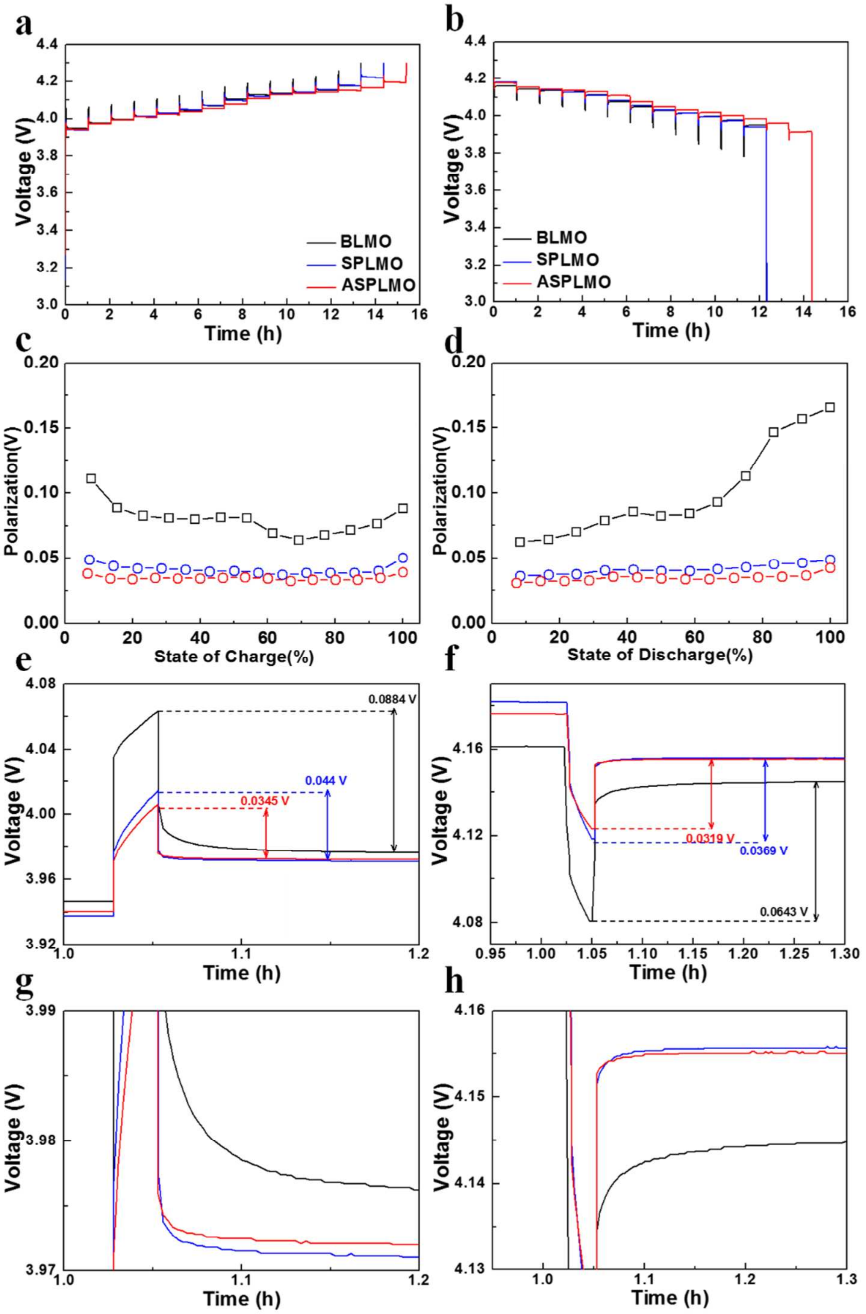

Figure S8. GITT potential responses during (a) charge and (b) discharge, polarization of BLMO, SPLMO and ASPLMO during (c) charge and (d) discharge. (e and f) expended images of the regions in (a and b), respectively. (g and h) expended images of the regions in (e and f), respectively.

Table S1. Representative rate performance of nanosized class materials from literature. AM, CM and BD are active material, conductive material and binder, respectively.

Material specification	Electrode composition (AM:CM:BD)	Particle Size	Practical capacity (mAh/g)	Performance	Refs
This work	80:10:10	Micron	119 (0.1C)	96.2% at 30C 92.7% at 100C 77.8% at 500C	-
$LiMn_2O_4$ Nanowires	75:17:8	Nano	116 (1C)	69% at 20C 50% at 30C	(1)
$LiMn_2O_4$ Nanoparticles	75:20:5	Nano	116 (0.1C)	81.1% at 100C	(2)
$LiMn_2O_4$ Nanoparticles	85:10:5	Nano	125 (0.5C)	96.8% at 10C 81.6% at 20C	(3)
$LiMn_2O_4$ Nanorods	70:20:10	Nano	127 (1C)	63% at 30C	(4)
$LiMn_2O_4$ Nanocones	70:20:10	Nano	127 (0.1C)	92.2% at 30C 77.5% at 50C	(5)
$LiMn_2O_4$ Nanorods	70:20:10	Nano	114 (0.5C)	88% at 10C 79.8% at 20C	(6)
$LiMn_2O_4$ Microcube	80:10:10	Micron	120 (0.1C)	84% at 10C 78.4% at 20C	(7)

References

1. Lee, H.-W.; Muralidharan, P.; Ruffo, R.; Mari, C. M.; Cui, Y.; Kim, D. K. *Nano Lett.* **2010,** 10, 3852-3856.
2. Kim, J.-S.; Kim, K.; Cho, W.; Shin, W. H.; Kanno, R.; Choi, J. W. *Nano Lett.* **2012**, 12, 6358-6365.
3. Arumugam, D.; Kalaignan, G. P. *Electrochim. Acta* **2010**, 55, 8709-8716.
4. Cheng, F.; Wang, H.; Zhu, Z.; Wang, Y.; Zhang, T.; Tao, Z.; Chen, J. *Energy Environ. Sci.* **2011,** 4, 3668-3675.
5. Hosono, E.; Kudo, T.; Honma, I.; Matsuda, H.; Zhou, H. *Nano Lett.* **2009,** 9, 1045-1051.
6. Xie, X.; Su, D.; Sun, B.; Zhang, J.; Wang, C.; Wang, G. *Chem. – Eur. J.* **2014,** 20, 17125-17131.
7. Lu, J.; Fan, X.; Zhou, C.; Liu, Z.; Zheng, F.; Lee, K. S.; Lu, L. *J. Electrochem. Soc.* **2016,** 163, A197-A202.